

NACA RM L52F12

9787



NACA

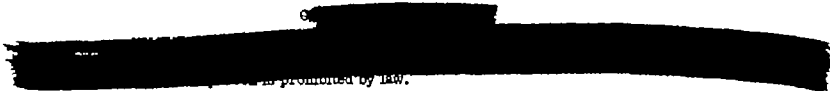


RESEARCH MEMORANDUM

INVESTIGATION OF VANES IMMERSSED IN THE JET
OF A SOLID-FUEL ROCKET MOTOR

By Leo V. Giladett and Andrew R. Wineman

Langley Aeronautical Laboratory
Langley Field, Va.



NATIONAL ADVISORY COMMITTEE
FOR AERONAUTICS

WASHINGTON

September 10, 1952

572 1 13



Classification cancelled (or changed to) Unclassified

By Nasa Tech Rb Announcements #116
(OFFICE USE ONLY - DO NOT CHANGE)

By 5 July 57

MG
(OFFICE USE ONLY - DO NOT CHANGE)

31 Mar 61
DATE

7

~~CONFIDENTIAL~~

NATIONAL ADVISORY COMMITTEE FOR AERONAUTICS

RESEARCH MEMORANDUM

INVESTIGATION OF VANES IMMERSED IN THE JET
OF A SOLID-FUEL ROCKET MOTOR

By Leo V. Giladett and Andrew R. Wineman

SUMMARY

In order to provide data for a jet-vane stabilization system, the characteristics of a particular vane configuration in the jet of a 6.25-inch Deacon solid-fuel rocket motor were determined from static tests. The vanes were oscillated during the test to provide comprehensive data over a range of deflection angles. The effects of the rocket jet on two vane materials, the aerodynamic characteristics of the vanes, and the influence of jet vanes on rocket-motor performance were determined.

Polished SAE 1020 steel and carbon-graphite vane materials were tested. The SAE 1020 steel vanes were considered to be satisfactory in all respects and may be incorporated, without change, into a stabilization system employing the 6.25-inch Deacon rocket motor.

Vane aerodynamic data are presented in both force and coefficient forms. Lift and hinge moments varied linearly with deflection angles through a range of -12.5° to 12.5° . A maximum lift of 76 pounds was obtained with hinge moments of less than 6 inch-pounds. Lift- and hinge-moment-curve slopes expressed as coefficients were constant at 0.0199 and -0.00060 per degree, respectively, for the duration of the tests. The center-of-pressure location was constant at 42.5 percent chord throughout the tests. A maximum drag of 75 pounds was not considered to be excessive for this application.

The effects of the jet vanes on rocket-motor performance are given as impulse losses. The measured impulse loss for four vanes, pulsed to $\pm 12.5^{\circ}$, was 3.63 percent of the rocket total impulse. If four vanes were at a maximum deflection throughout the test, the estimated impulse loss would be less than 4.50 percent; if at zero deflection, the impulse loss would be slightly greater than 3 percent.

~~CONFIDENTIAL~~

H. G. B. 177

INTRODUCTION

The forces available from deflecting a high-velocity jet can be utilized to provide stability and control for jet aircraft and rocket-powered missiles. Jet vanes may be used to an advantage when the dynamic pressure over the external lifting surfaces is low, occurring when the aircraft is at low velocities or high-altitude flight.

In the investigations made by the Pilotless Aircraft Research Division, aerodynamic research models are propelled in flight by solid-propellant rocket motors. In order to provide stability for models employing booster motors, large fixed fins are used. The design of these fins is complicated by problems involving aeroelasticity and flutter, resulting in fins having considerable weight and drag which reduces the rocket impulse available for accelerated flight. An analysis indicated that the fixed-fin booster could at best be only moderately efficient and an attempt should be made to find a more efficient system of stabilization.

The feasibility of deriving forces by the deflection of a portion of the rocket jet was reported for ground tests in reference 1. After this investigation, preliminary flight tests were made to determine the effectiveness of a complete fin-actuated jet-vane stabilization system. These tests were reported in reference 2 and the conclusion was made that this system possessed many advantages over the fixed fins. The jet-vane system was not only more effective at low speeds, but exhibited a markedly higher booster efficiency. These conclusions led to the initiation of an investigation into the application of the jet-vane system to the 6.25-inch Deacon rocket motor, large numbers of which are used as booster motors. This investigation required that a suitable jet vane be evolved and that the aerodynamic characteristics of the vanes be determined prior to their incorporation into a complete system.

Accordingly, a series of static tests of a particular vane configuration were made by using the 6.25-inch Deacon rocket motors, the results of which are reported in this paper. This information will apply to the design of a complete jet-vane stabilization system.

SYMBOLS

C_L	lift coefficient, $L/q_e S$
C_D	drag coefficient, $D/q_e S$

CONFIDENTIAL

C_h	hinge-moment coefficient, $H/q_e S_e$
L	lift of one vane, lb
D	drag of one vane, lb
H	hinge moment of one vane, in-lb
F_m	measured rocket thrust, lb
F	rocket thrust, $F_m + 2D_p + 2D_f$, lb
Y	total side force, lb
N	total yawing moment, in-lb
$C_{L\delta}$	rate of change of lift coefficient with vane deflection, $dC_L/d\delta$, per degree
$C_{h\delta}$	rate of change of hinge-moment coefficient with vane deflection, $dC_h/d\delta$, per degree
L_δ	rate of change of lift with vane deflection, $dL/d\delta$, lb/deg
H_δ	rate of change of hinge moment with vane deflection, $dH/d\delta$, in-lb/deg
t	time, sec
δ	vane deflection, deg
S	area of one vane, sq in.
b	vane span, in.
c	vane chord, in.
A	vane aspect ratio, b^2/S
M	Mach number
q	jet dynamic pressure, lb/sq in.
p	measured static pressure, lb/sq in.

~~CONFIDENTIAL~~

c.p. center of pressure, percent chord from the leading edge

I total impulse, $\int F dt$, lb-sec

Subscripts:

e rocket nozzle exit

a atmospheric

c head end of rocket chamber

n nozzle entrance of rocket chamber

p pulsed-jet vane

f fixed-jet vane

APPARATUS AND TESTS

Jet Vanes

A simple jet-vane configuration (fig. 1) was selected on the basis of successful tests which were reported in reference 2. The 6.19-inch diameter of the nozzle exit necessitated the use of relatively small vanes. Since maximum erosion was expected near the center of the jet where temperature and velocity were greatest, the span of the vane was limited to 1.25 inches. In order to obtain a reasonable lifting surface, the chord was fixed at 2 inches. Vane hinge axes were located at 30 and 40 percent of the chord. The aspect ratio of this plan form was 0.625. Other vane investigations reported in references 3 and 4 also used low-aspect-ratio vanes.

The requirement for a suitable jet-vane material is that it substantially retains its configuration throughout the burning time of the rocket, regardless of the aerodynamic loads imposed and the erosive conditions encountered in the jet. The vane materials must possess either high thermal conductivity and melting temperature or adequate heat-resisting properties. Polished SAE 1020 steel and carbon-graphite vane materials were tested. The selection of 1020 steel as a jet-vane material was influenced by the behavior of several metals exposed to a rocket jet (as reported in refs. 5 and 6). Carbon graphite, a commercially available product, has excellent heat-resisting properties in a reducing atmosphere (a deficiency of oxygen), a condition peculiar to the jet of the rocket motors used for these tests. For this particular jet-vane application, grade 15 carbon graphite with a skin treatment was recommended.

Thrust Stand and Vane Balance

The forces acting on the rocket motor and jet vanes are shown in figure 2. Thrust, side force, and yawing moment were measured with the three-component thrust stand. (See fig. 3.) The rocket motor was supported at two points as shown in figure 3(a). The rocket-head cap was made to be an integral part of the front support, whereas the nozzle end was held in rollers. These rollers permitted axial vibration and expansion while restraining vertical and side-ways motion. The front support incorporated electric strain-gage beams for measurement of thrust. Side force and yawing moment were measured by electric strain-gage beams in both front and rear supports. Yawing moment was measured about the yaw center as shown in figure 2 and thrust was calibrated with the instrument shown in figure 3(b). A steel cable, loaded in tension by a hydraulic power unit, applied force along the rocket axis. The applied loads were established by a ring dynamometer integral within the cable. Side force and yawing moments were calibrated by the application of loads established by a ring dynamometer.

The jet-vane balance (fig. 4) incorporated electric strain-gage beams to measure vane lift, drag, and hinge moment. These beams were calibrated with dead weights. The vane deflection indicators were calibrated (fig. 4(b)) by the use of a pointer replacing the jet vane and a graduated sector mounted on a frame fitted to the nozzle. The nozzle entrance, nozzle exit, and head pressures were measured with electric strain-gage type of pickups.

Rocket Motors

The rocket motors used for the tests were 6.25-inch Deacon motors which have a single, internal burning, star-perforated grain. A steel pressure take-off chamber was assembled between the heat-transfer coupling and the nozzle as shown in figure 5. Nozzle-entrance static pressure was taken off the wall of this chamber. In order to promote smooth burning, 90-inch resonance rods were used instead of the standard 72-inch rods. The standard igniters were replaced with NACA igniters. Provisions were made for static-pressure take-offs at the head cap and nozzle exit. A bearing band was clamped around the rocket chamber at the thrust-stand rear support in order to distribute the side-force loads.

The 6.25-inch Deacon motor is made in two types, 3.5 ES-5700 and 3.5 DS-5700. During the investigation, the use of the 3.5 ES-5700 Deacon motor was discontinued and the 3.5 DS-5700 Deacon motor was adopted in its place; accordingly, a 3.5 DS-5700 Deacon motor was used in test 3. Nominal rocket data for the 6.25-inch Deacon motors are shown in table I.

Jet-Vane Testing Assembly

The jet-vane testing apparatus consisted of two principal parts - a vane support assembly and a vane pulsing mechanism. The vane support assembly consisted of a collar clamped around the rocket heat-transfer coupling and four vane support arms attached to the collar 90° apart. (See fig. 4(b).) Two opposite vanes were positioned at zero deflection relative to the rocket jet. The pulsed vanes (fig. 4(a)) were held in a manner to permit rotation about a common axis perpendicular to the jet. The angular deflections of the vanes were obtained by means of slide-wire potentiometers. The arm supporting one of the pulsed vanes incorporated an electric strain-gage balance to measure lift, drag, and hinge moment. The pulsing mechanism (fig. 4(a)) consisted of an electric motor with a speed reducer mounted in a rigid steel frame fixed to the thrust-stand rails. Rotation was transmitted from the motor to the main shaft through a vee belt. Identical linkages converted the rotary motion of the main shaft to an unsymmetrical oscillating motion of the two vane shafts. The vane shafts incorporated flexible and sliding joints, preventing extraneous forces from influencing the vane data. No-load maximum vane deflections were $\pm 14^\circ$.

Instrumentation

Forces, moments, and pressures were measured with strain-gage pickups, whereas vane deflections were determined by the use of slide-wire pickups. By the use of potentiometers these measurements were completed through galvanometer elements of a recording oscillograph which yielded continuous time histories of the following: vane deflections, lift, drag, hinge moment, thrust, side force, yawing moment, head pressure, nozzle entrance pressure, nozzle exit pressure and ignition delay. The calibration of the preceding quantities was linear with trace deflections producing constant calibration factors. With the exception of side force and yawing moment, the data obtained from the oscillograph records have been found to be accurate within ± 2 percent of full-scale trace deflections.

Two 16-millimeter high-speed motion-picture cameras photographed the tests in color. These photographs, in addition to visual observations, provided qualitative data.

Tests

Three tests were made in this investigation. During the tests, the vanes were pulsed approximately $\pm 12.5^\circ$. The time for one cycle was approximately 1.76 seconds in test 1, 0.88 second in test 2, and

~~CONFIDENTIAL~~

0.44 second in test 3. The vane-hinge axes were 30-percent chord in tests 1 and 2 and at 40 percent chord in test 3. The position of the vanes, with respect to the rocket nozzle, was maintained as shown in figure 5(a) for all tests.

In test 1, the two pulsed vanes were carbon graphite, whereas the fixed vanes were steel. An Inconel shield was attached to the upper vane to protect the vane balance. In test 2 the upper pulsed vane was steel and the lower pulsed vane was carbon graphite. The fixed vanes were also one steel and one carbon graphite. In test 3, all four vanes were steel.

RESULTS AND DISCUSSION

Quantitative and qualitative information was obtained from all the tests. The behavior of the two vane materials in the rocket jet was observed. The aerodynamic characteristics of one of the vanes were determined, and the effects of the vanes on the rocket performance were found.

Jet Vanes

In test 1, pulsed vanes were grade 15 carbon graphite and the stationary vanes were SAE 1020 steel. Despite the fact that it was impossible to calculate the strength of either steel or carbon graphite at elevated temperatures (stagnation temperature varying from 3600° to 4200° R), it was anticipated that the carbon graphite would be more suitable for the test than SAE 1020 steel because of its better heat-resisting properties. The lower vane, which was constructed of carbon graphite, was broken off immediately upon ignition of the rocket motor. This vane is shown in position in figure 6(a) and also shown second from the left in figure 7(a). The fracture exposed the untreated interior of the vane to the action of the jet; however, little erosion of the stub was observed. No conclusion could be made as to the erosive resistance of the carbon graphite since the vane stub was near the outer boundaries of the jet. The upper vane, also carbon-graphite, was broken by the balance shield which warped into the jet near the end of the test. It is shown as the extreme left vane in figure 7(a). A study of the motion pictures of the test failed to reveal any excessive erosion of this vane prior to the fracture. The steel vanes were slightly eroded at the tip of the leading edge. (See fig. 7(a).) A slight oxidation at the junction of the vane leading edge and end plate occurred on all vanes in test 1. This phenomenon was more pronounced in the carbon-graphite vanes than on the steel, since steel oxidizes less readily at these temperatures. The SAE 1020 steel vane material appeared completely satisfactory, although the effect of being pulsed in the jet was not determined.

~~CONFIDENTIAL~~

Accordingly, in test 2, both SAE 1020 steel and carbon-graphite vanes were pulsed in the jet. An SAE 1020 steel vane was used on the vane balance, since it was more likely to last the duration of the test. The excellent condition of SAE 1020 steel vanes from test 1 warranted their reuse in test 2. The lower pulsed vane (fig. 6(b)) was carbon graphite and was noticeably more eroded than the fixed carbon-graphite vane adjacent to it (as shown by the two vanes on the left of fig. 7(b)). As a comparison of the erosion between carbon graphite and steel, the two vanes on the right of the same figure are the pulsed and fixed steel vanes; these vanes did not exhibit any additional erosion due to motion in the jet. It was evident that the steel vanes were less eroded in all cases than the carbon-graphite vanes. It was also found that the carbon-graphite vanes were subject to chipping and breaking due to handling, an indication that steel vanes were more reliable.

All four vanes used in test 3 were SAE 1020 steel. The second test indicated that the vane hinge moments were larger than desired. In order to reduce these hinge moments, the vane hinge axis was shifted from 30 to 40 percent of the chord. Calculations indicated that the stagnation temperature of the jet of the 3.5 DS-5700 rocket motor used in test 3 was 3584° R, which was considerably lower than the 4219° R temperature encountered in tests 1 and 2 in which the 3.5 ES-5700 rocket motor was used. The vanes used in test 3, all equally eroded, are shown in figure 7(c). The pulsed vanes, numbered 1 and 3, and the fixed vanes, numbered 2 and 4, suffered even less erosion than the vanes of test 1. Although the lower stagnation temperature was known to reduce the erosion, any effect of the change in jet-gas composition could not be determined. The fixed vanes exhibited distinct flow patterns etched in the thin coating of combustion products deposited on all vanes. The patterns were not as clearly defined on the pulsed vanes. These patterns were of no quantitative value, but they did illustrate the complexity of the jet stream across the vanes.

High temperatures attending detached shock waves off the vane leading edge caused local burning of the rocket nozzle in all tests. (See fig. 6(b).) It was assumed that this did not affect the operation of the rocket or the jet vanes.

Aerodynamic Characteristics

Vane-balance data.— The data furnished by the vane balance in test 3 are shown in figure 8. An inspection of the shape of the time history of vane deflection indicates that δ increases from -12° to 12° in 0.15 second and decreases from 12° to -12° in 0.13 second. This unsymmetrical pulse provided data for different deflection rates. The deflection-angle amplitudes were not constant because of the strain of the pulsing mechanism

under load. Seven complete cycles of data were obtained in this test including the lift, drag, and hinge moment of the vane. Positive and negative signs were assigned to all data for convenience in correlation and identification only. Accordingly, for purposes of quantitative evaluation, data were used without regard to sign. At maximum deflection angles, vane lift varied from 62 to 76 pounds, hinge moment, from 3.9 to 5.7 inch-pounds, and drag, from 65 to 75 pounds. Drag at zero deflection angles varied from 48 to 57 pounds.

Thrust-stand data.- Thrust-stand data consisting of time histories of yawing moment, side force, rocket head pressure, nozzle-entrance pressure, and measured thrust are shown in figure 9. No quantitative comparison could be made between the vane-balance data and thrust-stand data since the side force and yawing moment experienced severe high-amplitude oscillations at low frequency. Therefore, the side-force and yawing-moment data were presented as faired values to be used only to indicate the approximate forces to which the rocket motor was subjected.

Aerodynamic forces.- The lift, drag, and hinge-moment data are plotted against the deflection angle in figure 10 for a typical cycle occurring from 2.04 to 2.46 seconds in test 3. The lift-curve slope was 5.65 pounds per degree for decreasing δ and 6.05 pounds per degree for increasing δ . Similarly, hinge-moment slopes were -0.36 and -0.43 inch-pound per degree, respectively. This difference is mainly due to variation in dynamic pressure. The minimum drag of 54 pounds occurred at zero deflection angle and the drag rise due to lift was a maximum of 20.8 pounds for 12° deflection. Both lift and hinge moment for this deflection range were linear. The linearity coupled with the good lift-curve slope and low hinge moments that were experienced make this vane suitable as a means of control. Drag characteristics are not objectionable for this application, since a thinner section would probably erode excessively and fail structurally. The variation of lift- and hinge-moment-curve slopes with time is given in figure 11. These slopes are plotted at times when deflection angles were zero. Lift-curve slopes varied from 4.8 to 6.05 pounds per degree, whereas the hinge-moment slope was practically constant at -0.35 inch-pound per degree throughout the test.

Aerodynamic coefficients.- In order to convert the vane forces to coefficient form, an acceptable method for the determination of dynamic pressure was needed. Since it was not possible to calculate the actual dynamic pressure of the complex flow field across the vanes, it was necessary to compute the average dynamic pressure at the nozzle exit $\frac{1}{16}$ -inch upstream of the vane leading edge, by the method shown in the appendix. This method requires time histories of measured thrust and nozzle-entrance pressure (fig. 9), and vane drag (fig. 8). The time

history of minimum or fixed vane drag is presented in figure 12 together with the time history of thrust computed by equation (6) of the appendix. Nozzle-exit pressure is not presented. The instruments which were used measured only positive gage pressures. An analysis of the record indicated that for part of the test the exit pressure was actually negative. For the portion of the record which was valid, the static-pressure ratio p_n/p_e was found. This experimental ratio was equal to the theoretical value of 61 calculated by equation (5) of the appendix. Accordingly, this ratio together with the time history of p_n furnished values of p_e required by equation (3) of the appendix. The time history of q_e obtained by this method is shown in figure 12.

The lift, drag, and hinge-moment data were converted to coefficient form from test 3. These coefficients are plotted against the deflection angle in figure 13 for the typical cycle. The slope of the lift-coefficient curve was 0.0191 per degree for both increasing and decreasing vane deflections. Similarly, hinge-moment curve slopes were -0.00058 per degree. Linearity of both lift and hinge-moment coefficients was good. Time histories of $C_{L\delta}$ and $C_{h\delta}$ are given in figure 14. Lift-curve slopes expressed in coefficient form do not exhibit any dependence upon deflection rates. Because of the variation of q_e with time, $C_{L\delta}$ and $C_{h\delta}$ remain essentially constant at 0.0199 and -0.0006 per degree, respectively, throughout the test. This value of $C_{L\delta}$ was higher than the value of 0.0169 per degree calculated from reference 4 for a rectangular flat plate with an aspect ratio of 0.625 and a Mach number of 3.2. This phenomenon of experiment being greater than theory was also noted in reference 2.

The variation of center of pressure with deflection angle for tests 2 and 3 is given in figure 15. The location appears to be independent of the deflection angle with a value of 42.5 percent of chord for both tests. The center of pressure compares with the theoretical value of 43.5 percent chord which was determined by reference 8.

Rocket-Motor Performance

The performance of a rocket motor is generally indicated by the total impulse I which may be evaluated by taking the integral of the thrust-time history. The impulse which was attributable to the vane drag during the test is similarly the integral of the drag time history. The rocket total impulse of test 3 was evaluated as 17,225 pound-seconds and was obtained by integration of the time history of thrust. The measured impulse loss in test 3 was 625 pound-seconds, or 3.63 percent of total impulse.

From information obtained in this test, it was possible to estimate the penalties imposed by these jet vanes on the total impulse of the rocket. The greatest possible impulse loss would have occurred if all four vanes had been at a maximum deflection angle for the entire test. The loss due to one such vane (190 lb-sec) is the integral of the value of D_{max} time history which was obtained by fairing points of maximum D_p . (See fig. 12.) Thus, the maximum loss for four vanes would have been 760 pound-seconds, or 4.40 percent of the rocket total impulse. Conversely, the minimum loss for one vane (140 lb-sec) is the integral of the D_{min} time history. Hence, the minimum loss for four vanes would have been 560 pound-seconds, or 3.13 percent of the rocket total impulse.

CONCLUSIONS

The characteristics of a low-aspect-ratio vane immersed in the jet of a 6.25-inch Deacon solid-fuel rocket motor were determined from a series of static tests. Vane aerodynamic forces and coefficients were ascertained. The losses in rocket performance due to the vanes as well as the effects of the rocket jet on two vane materials, yielded the following conclusions:

1. Jet vanes: SAE 1020 steel vanes proved satisfactory for this particular application. Grade 15 carbon-graphite vanes eroded excessively and were found to be unreliable in operation.

2. Aerodynamic characteristics: The vanes were oscillated in the jet to deflection angles of $\pm 12.5^\circ$. Lift and drag forces up to 76 pounds were obtained with hinge moments of less than 6 inch-pounds. Both lift and hinge moment were observed to be linear. The lift-curve slope varied from 4.8 to 6.1 pounds per degree, whereas hinge-moment slope was practically constant at -0.35 inch-pound per degree. Lift and hinge-moment coefficients, based on dynamic pressure at the nozzle exit, yielded constant slopes of 0.0199 and -0.0006 per degree, respectively. The center of pressure was found to be at 42.5 percent chord.

3. Rocket motor performance: The measured impulse loss for four vanes was 3.63 percent of the rocket total impulse. It was estimated that the impulse losses for this installation would always be between 3 and $4\frac{1}{2}$ percent.

On the basis of these results, it is concluded that these jet vanes are suitable for inclusion into a jet-vane stabilization system employing the 6.25-inch Deacon rocket motor.

Langley Aeronautical Laboratory
National Advisory Committee for Aeronautics
Langley Field, Va.

APPENDIX

DETERMINATION OF DYNAMIC PRESSURE AT NOZZLE EXIT

A method for calculating dynamic pressure at the nozzle exit was developed in reference 1. For small divergence angles, the relation is,

$$q_e = \frac{1}{2} \left[\frac{\bar{F}}{A_e} - (p_e - p_a) \right] \quad (1)$$

A correction factor λ must be applied for large divergence angles α which were given in reference 9 as

$$\lambda = \frac{1}{2}(1 + \cos \alpha) \quad (2)$$

The value of λ for the 30° divergence angle of the tests was 0.933. Equation (1) after being corrected for large divergence angles is now

$$q_e = \frac{1}{2\lambda} \left[\frac{\bar{F}}{A_e} - (p_e - p_a) \right] \quad (3)$$

Time histories of \bar{F} and p_e are required for the evaluation of q_e by equation (3).

If exit pressure p_e is not recorded, it must be calculated by other means. The pressure ratio p_e/p_{sn} as a function of area ratio A_e/A_t and specific heat ratio γ is given in reference 10 as

$$\frac{A_e}{A_t} = \left(\frac{\gamma - 1}{2} \right)^{1/2} \left(\frac{2}{\gamma + 1} \right)^{\frac{\gamma+1}{2(\gamma-1)}} \left(\frac{p_{sn}}{p_e} \right)^{1/\gamma} \left[1 - \left(\frac{p_e}{p_{sn}} \right)^{\frac{\gamma-1}{\gamma}} \right]^{-1/2} \quad (4)$$

The gas velocity at the nozzle entrance was considered to be sufficiently low to assume that the stagnation pressure p_{sn} was for all practical purposes equal to the static pressure p_n . Equation (4) thus becomes

$$\frac{A_e}{A_t} = \left(\frac{\gamma - 1}{2}\right)^{1/2} \left(\frac{2}{\gamma + 1}\right)^{\frac{\gamma+1}{2(\gamma-1)}} \left(\frac{p_n}{p_e}\right)^{1/\gamma} \left[1 - \left(\frac{p_e}{p_n}\right)^{\frac{\gamma-1}{\gamma}}\right]^{-1/2} \quad (5)$$

The values of pressure ratio obtained from equation (5) accurately duplicate experimental results. The exit pressure may now be evaluated from measured values of nozzle-entrance pressure and the pressure ratio p_n/p_e obtained from equation (5). If p_e is less than atmospheric pressure p_a , the nozzle, by definition, is overexpanded. Since it is known that the jet stream separates from the nozzle wall at a value of p_e approximately equal to 5 pounds per square inch absolute, the dynamic pressure should be calculated for the portions of the test where p_e is greater than 5 pounds per square inch absolute.

The measured thrust was less than that of similar rockets without jet vanes. It was assumed that this difference was due to the drag of the jet vanes which were attached to the rocket motor. The thrust F is the jet thrust of the rocket motor with no jet vanes present, whereas the measured thrust F_m is F reduced by jet-vane drag. This relation may be expressed as the following:

$$\begin{aligned} F_m &= F - (2D_p + 2D_f) \\ F &= F_m + (2D_p + 2D_f) \end{aligned} \quad (6)$$

The drag of the pulsed vane D_p and the measured thrust F_m are recorded against time during the test. The time history of the drag of the fixed vane D_f may be obtained by fairing points of minimum drag D_{min} from the time history of D_p . Instantaneous values of F may, therefore, be calculated for use in equation (3).

REFERENCES

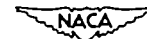
1. Bond, Aleck C.: Experimental Investigation of a Flat-Plate Paddle Jet Vane Operating on a Rocket Jet. NACA RM L50I20, 1950.
2. Wineman, Andrew R.: Preliminary Investigation of a Fin-Actuated Jet-Vane Control System for Stabilization of Rocket-Powered Models. NACA RM L50K17, 1951.
3. Friedman, Henry: Summary Report on A-4 Control and Stability. Summary Rep. F-SU-2152-ND, Air Materiel Command, U. S. Army Air Forces, June 1947.
4. Powell, W. B.: Experimental Investigation With Jet Control Vanes. Progress Rep. No. 4-30, Jet Propulsion Lab., C.I.T., 1948.
5. Anon.: Combined Bimonthly Summary No. 11. Jet Propulsion Lab., C.I.T., May 1949.
6. Anon.: Combined Bimonthly Summary No. 19. Jet Propulsion Lab., C.I.T., Sept. 1950.
7. Anon.: Rocket Fundamentals. OSRD 3992, ABL-SR4, NDRC, Div. 3, Sec. H, 1944.
8. Piland, Robert O.: Summary of the Theoretical Lift, Damping-in-Roll, and Center-of-Pressure Characteristics of Various Wing Plan Forms at Supersonic Speeds. NACA TN 1977, 1949.
9. Sutton, George P.: Rocket Propulsion Elements. John Wiley and Sons, Inc., 1949.
10. Wimpres, R. N.: Internal Ballistics of Solid-Fuel Rockets. McGraw-Hill Book Co., Inc., 1950.

TABLE I

NOMINAL ROCKET DATA FOR 6.25-INCH DEACON MOTOR

	3.5 ES-5700	3.5 DS-5700
Powder type	H-9	OIY
Powder weight, lb	100	96.7
Burning time, 77° F, sec	2.89	2.62
Average thrust, 77° F, lb	6500	6424
Average pressure, 77° F, psi	1000	1092
Total impulse, 77° F, lb-sec	20,000	17,720
Nozzle-divergence angle, deg	30	30
Nozzle-throat diameter, in.	2.426	2.275
Nozzle-exit diameter, in.	6.188	6.188
Area ratio, A_t/A_e	0.154	0.135
Specific-heat ratio, γ	1.252	1.255
^a Exit temperature, T_e , deg R	1914	1554
^a Exit velocity, V_e , ft/sec	7099	6636
^a Exit Mach number, M_e	3.10	3.20
^a Pressure ratio, p_n/p_e	51	61

^aThe conditions of the jet at the nozzle exit were calculated by the method of appendix 8 (ref. 7) and isentropic flow relations.



~~CONFIDENTIAL~~

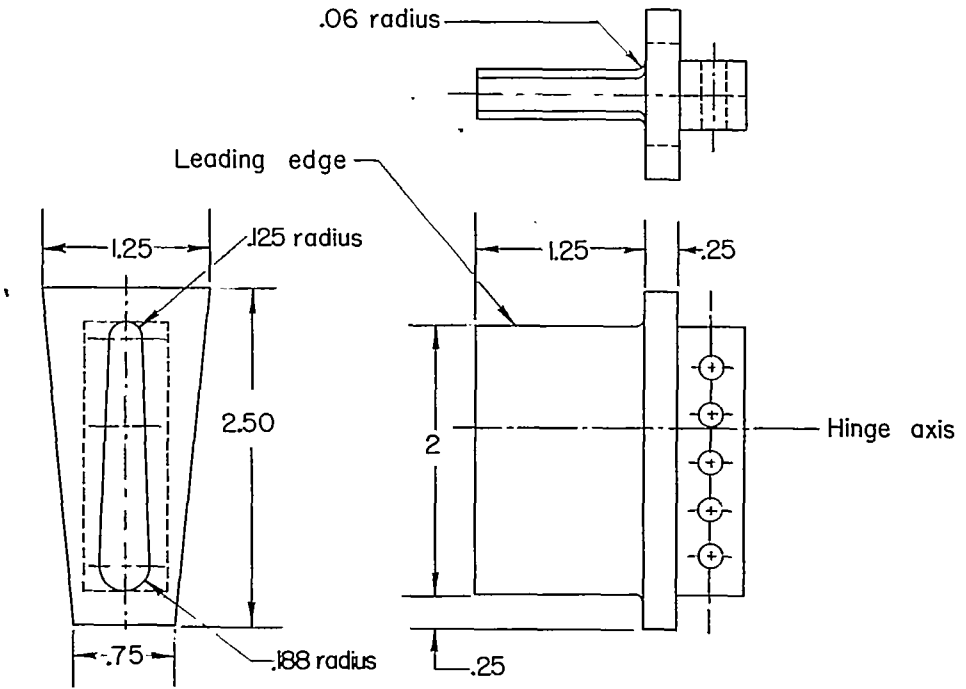
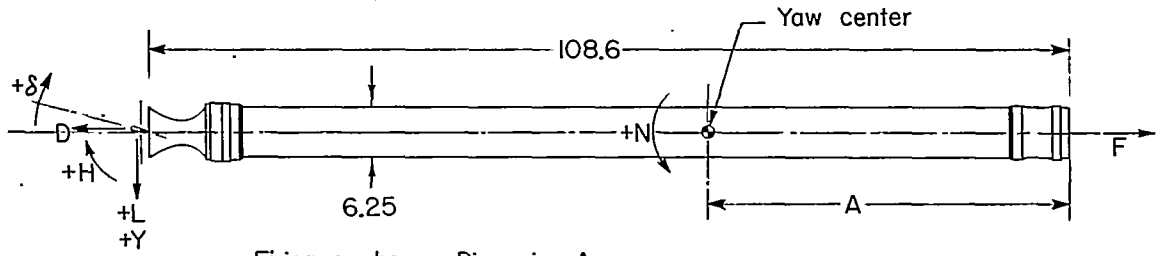


Figure 1.- Jet vane. All dimensions in inches.

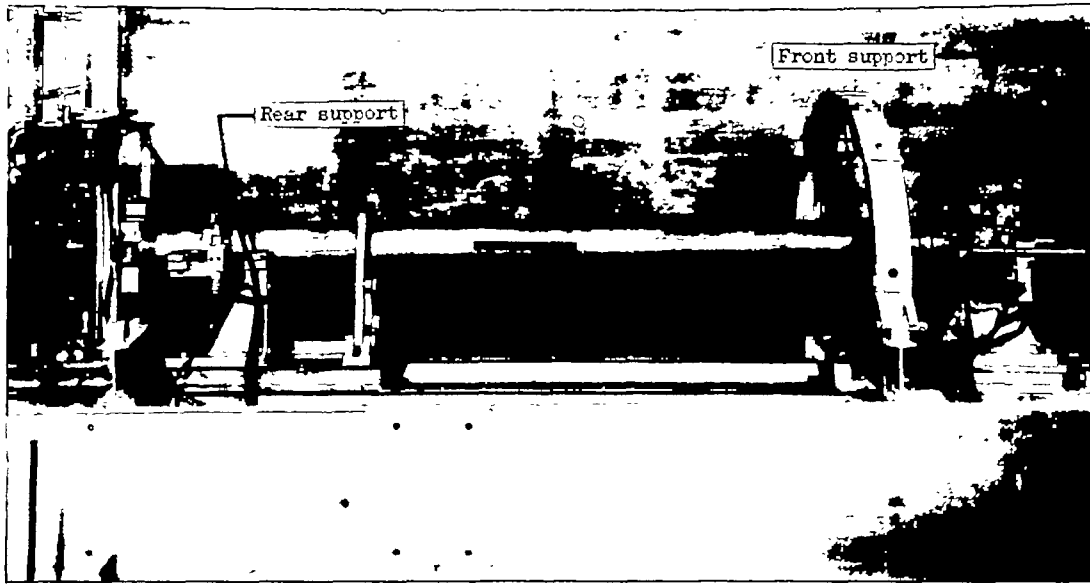


Firing number	Dimension A
1	420
2	420
3	38.7

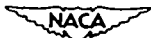


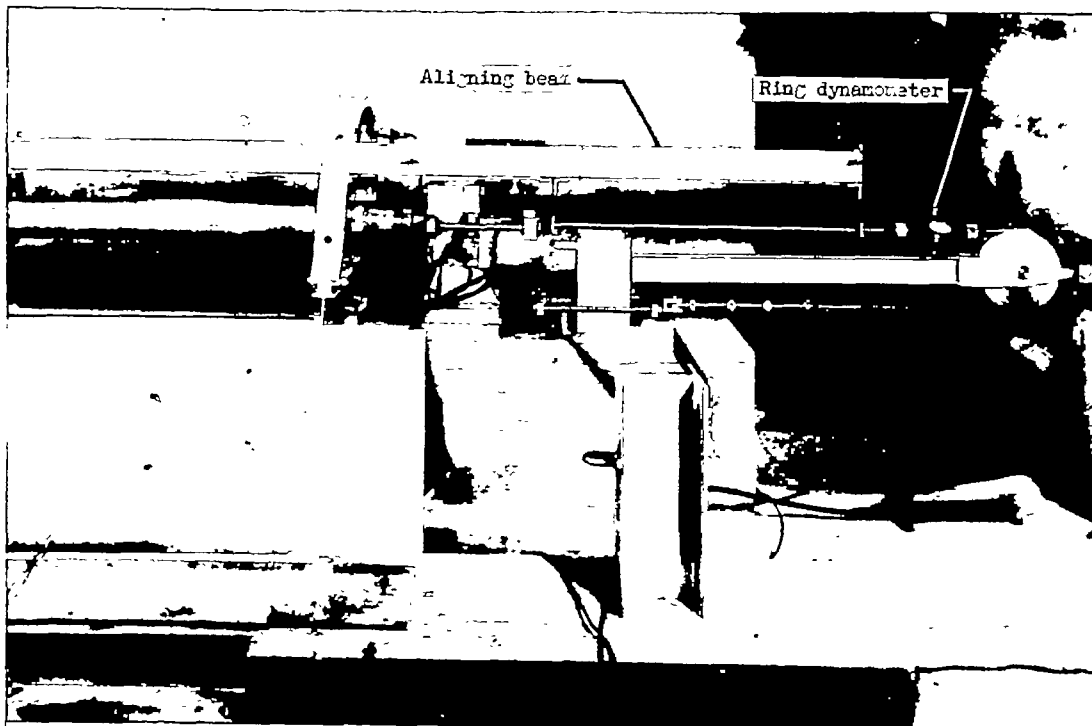
Figure 2.- Sketch of rocket motor showing direction of forces, moments, and deflections. All dimensions in inches.

~~CONFIDENTIAL~~



(a) Side view.


 L-69185.1



(b) Thrust alignment and calibration apparatus.

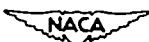
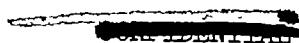
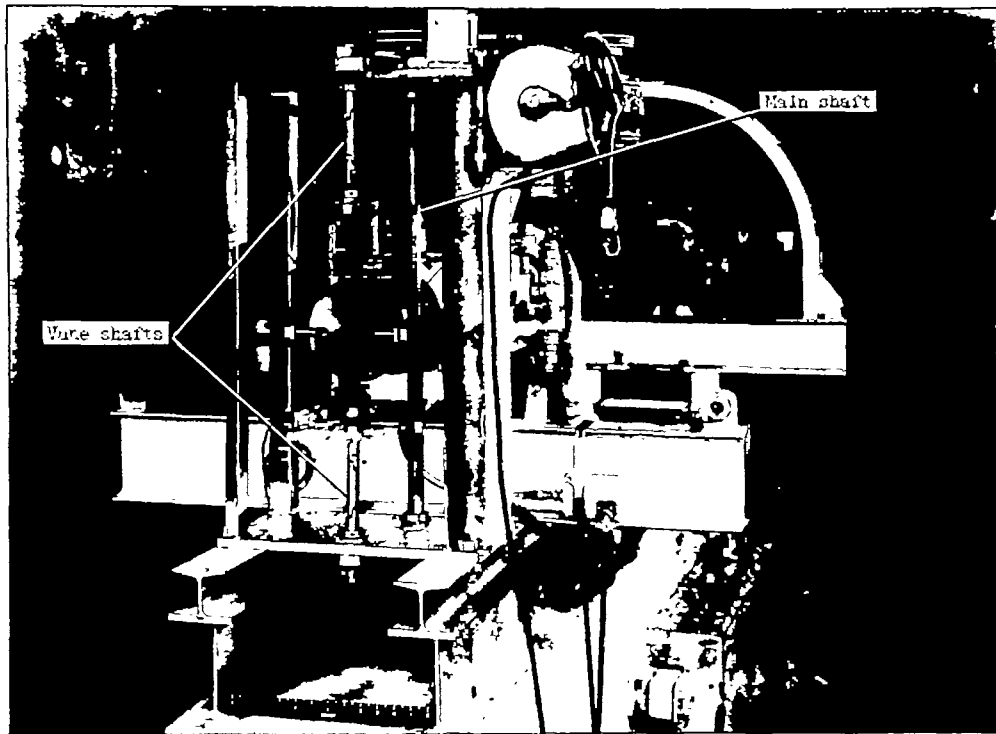


Figure 3.- Rocket thrust stand.

L-69184.1

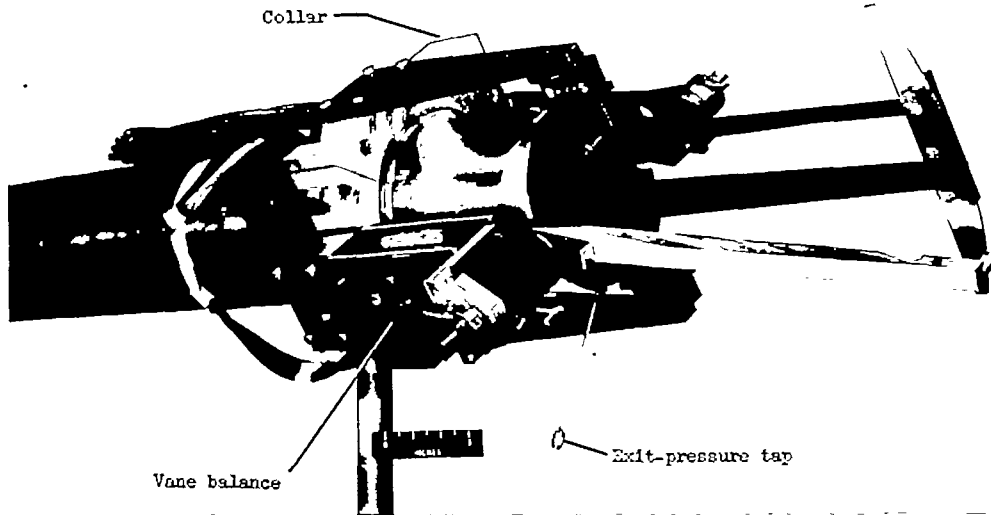




(a) Vane support assembly and pulsing mechanism in place on rocket thrust stand.



L-69183.1

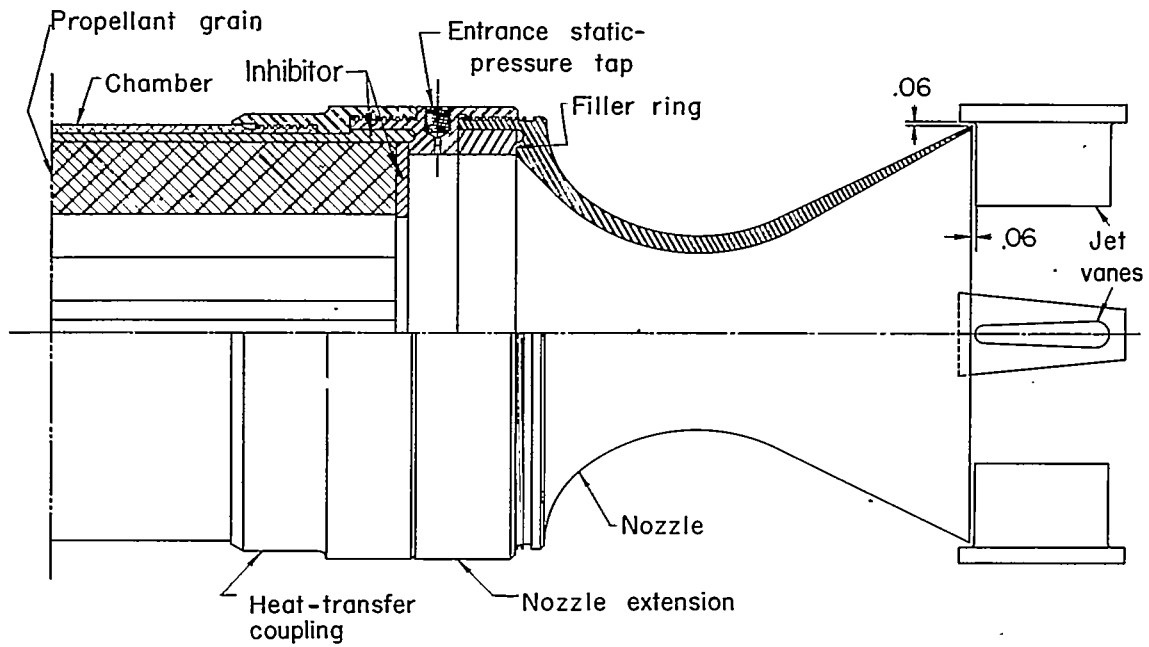


(b) Jet-vane balance and support assembly showing method of vane deflection calibration.

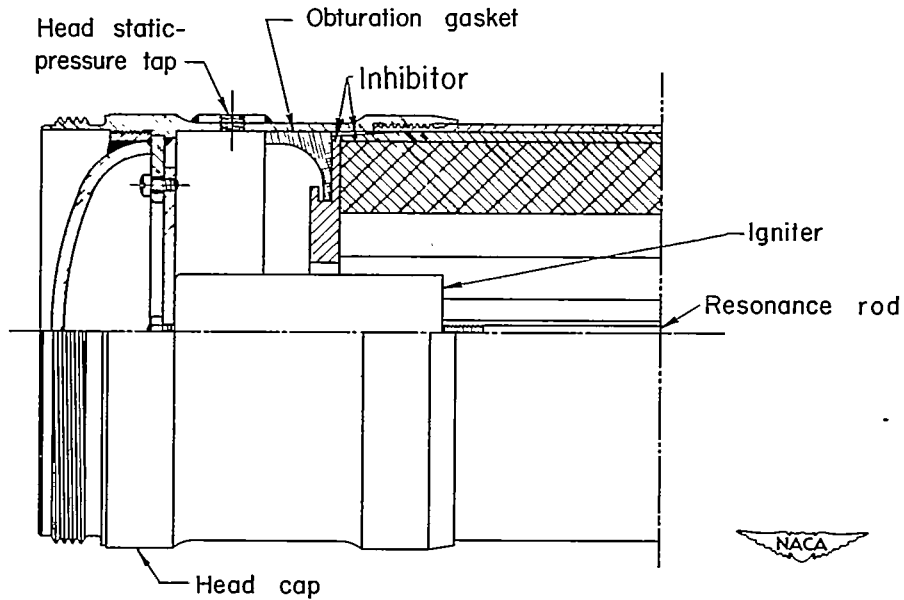


L-67694.1

Figure 4.- Jet-vane testing apparatus.

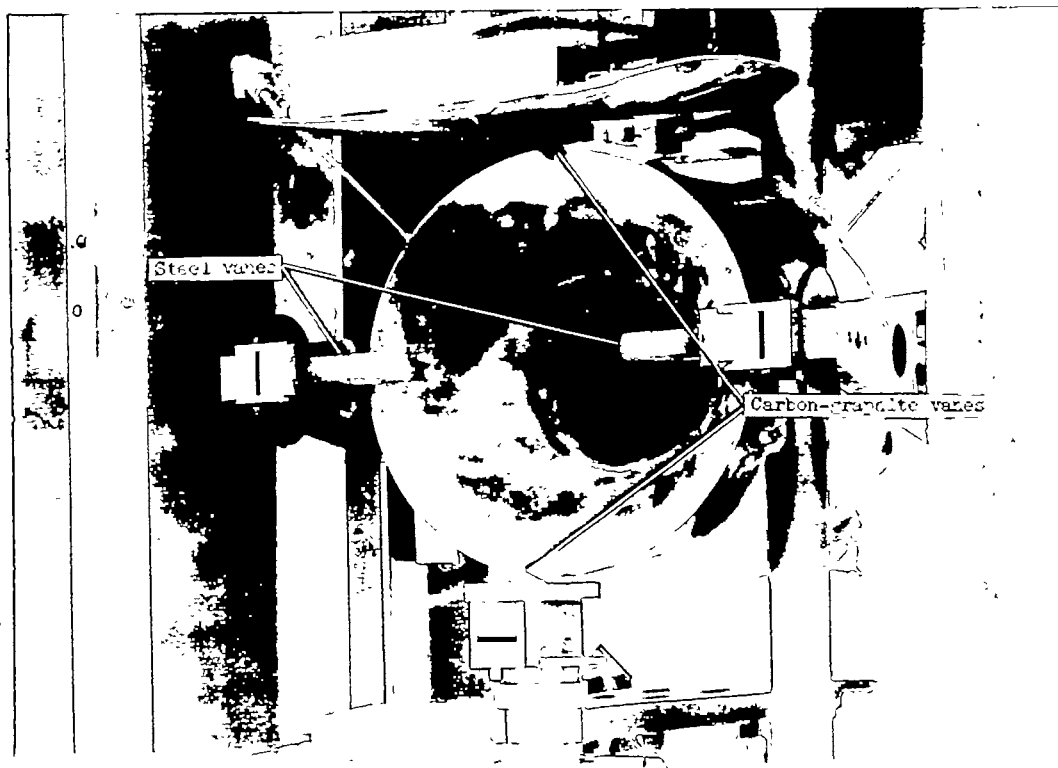


(a) Nozzle end.



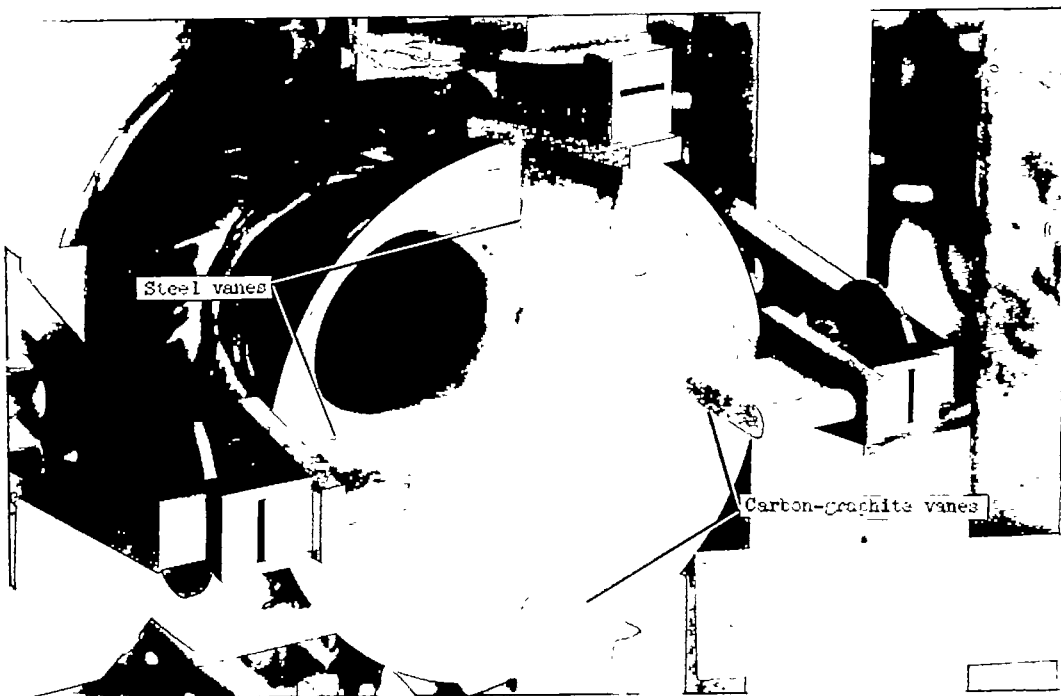
(b) Head end.

Figure 5.- Details of rocket-motor assembly showing location of pressure taps and jet vanes. All dimensions in inches.



(a) Test 1.

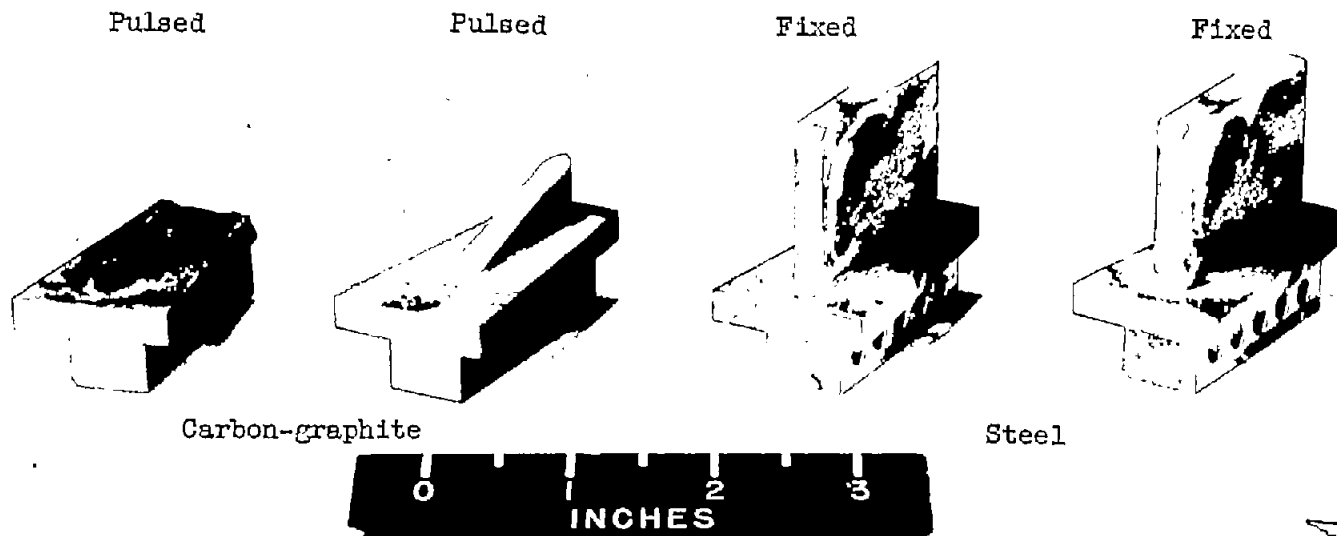

 L-69193.1



(b) Test 2.



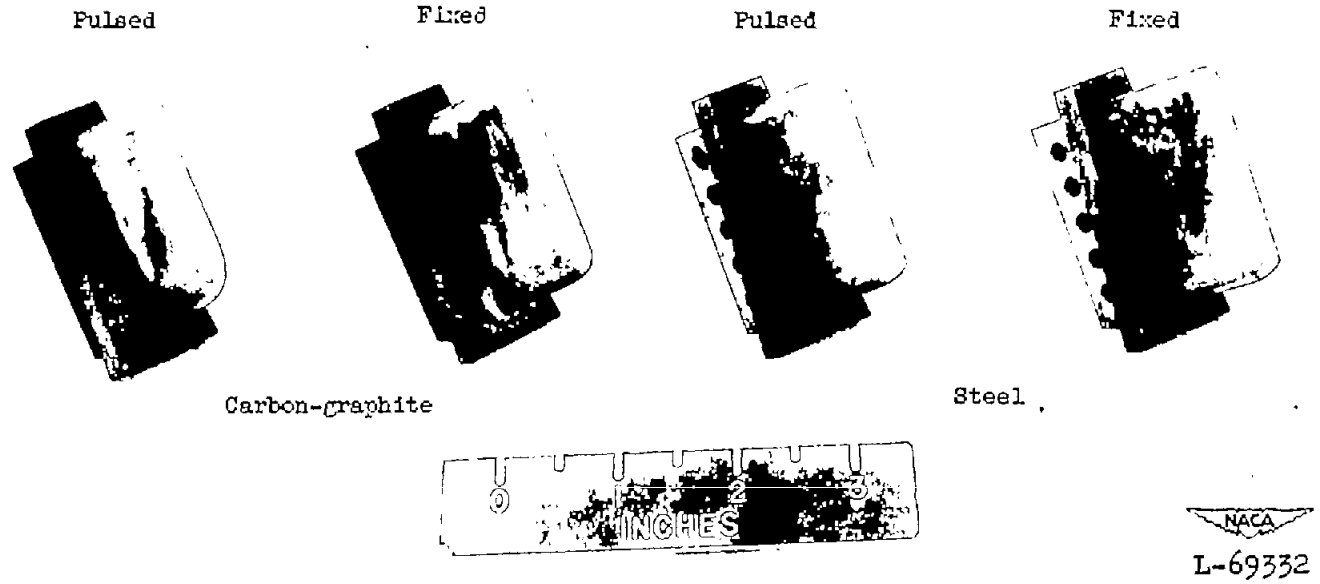
Figure 6.- Rocket nozzle and jet vanes after firing. L-69272.1



NACA
L-69190

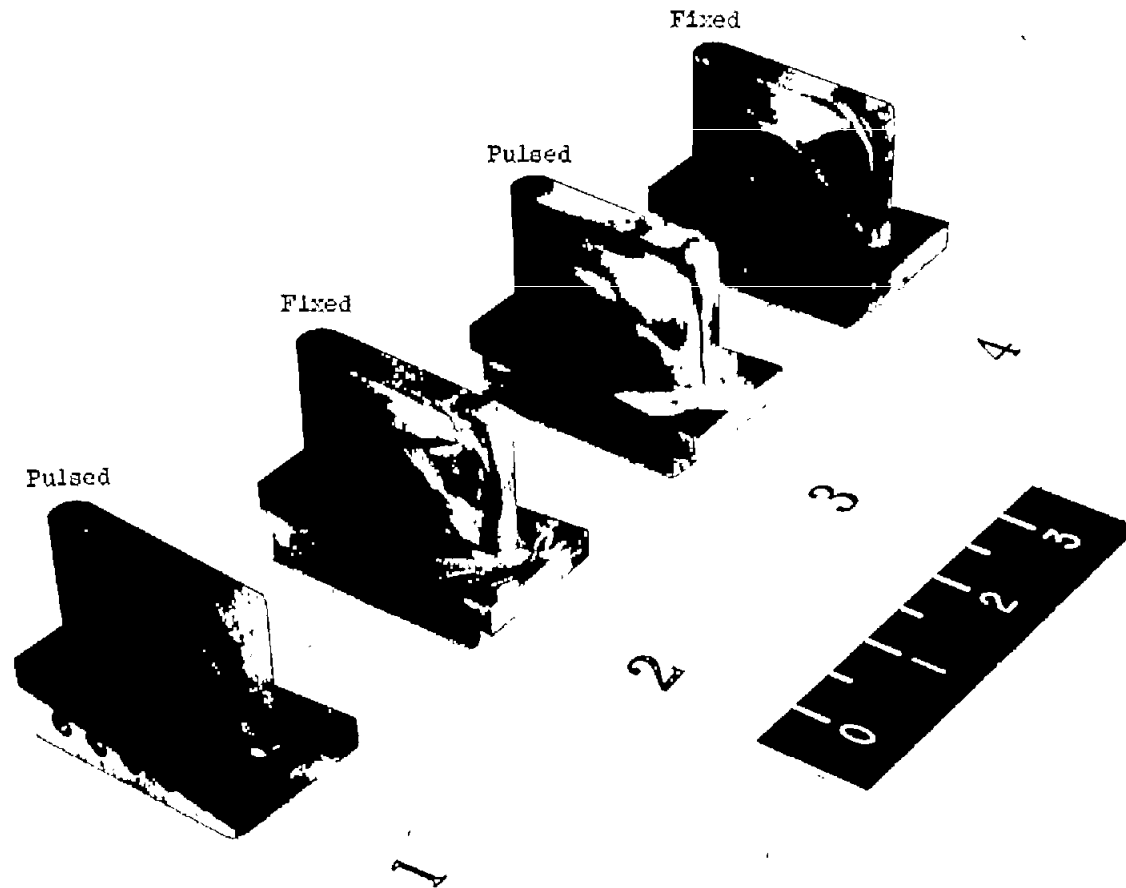
(a) Test 1.

Figure 7.- Jet vanes after firing.



(b) Test 2.

Figure 7.- Continued.



(c) Test 3, all vanes steel.

Figure 7.- Concluded.

NACA
L-72305

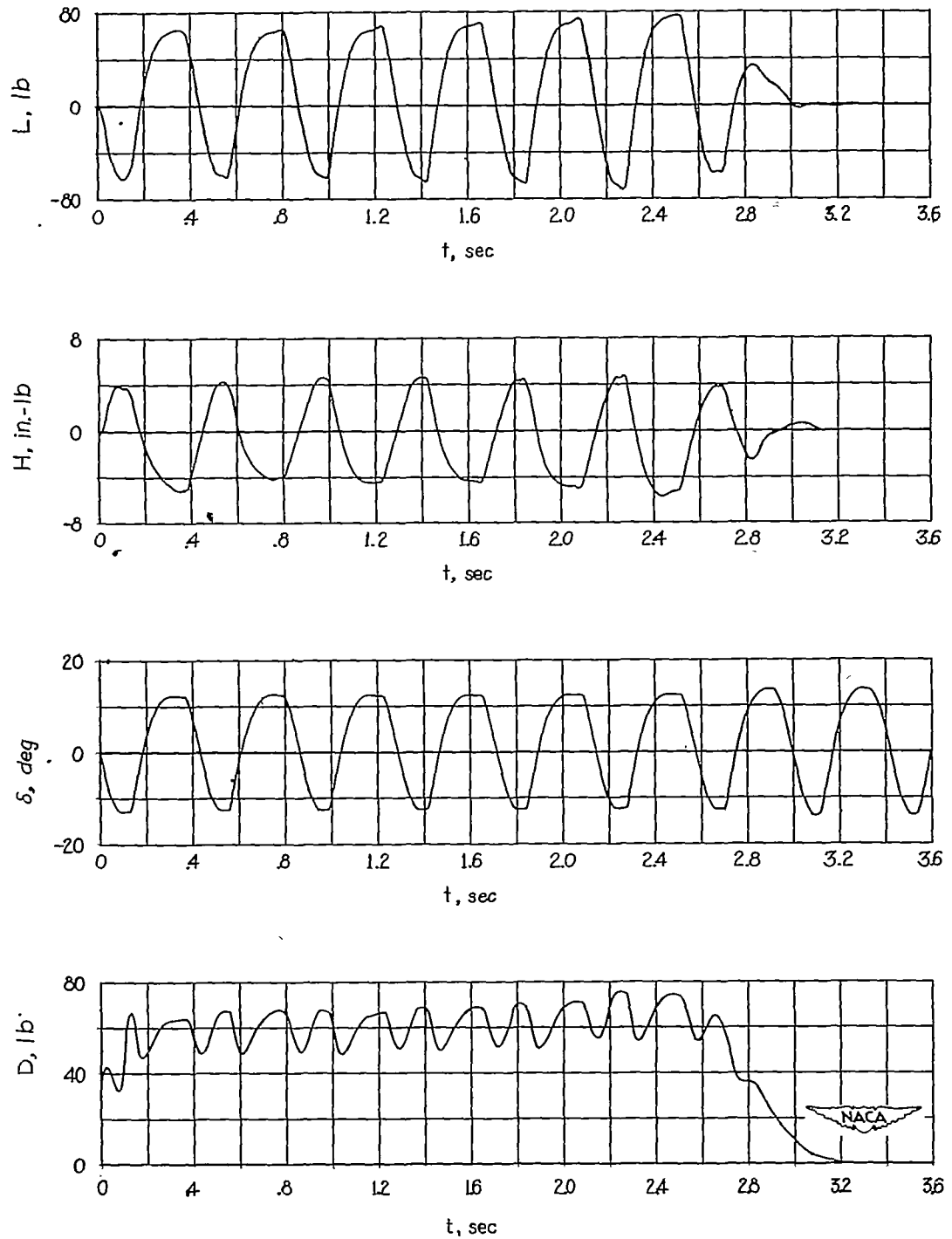


Figure 8.- Time history of vane-balance data obtained from test 3.

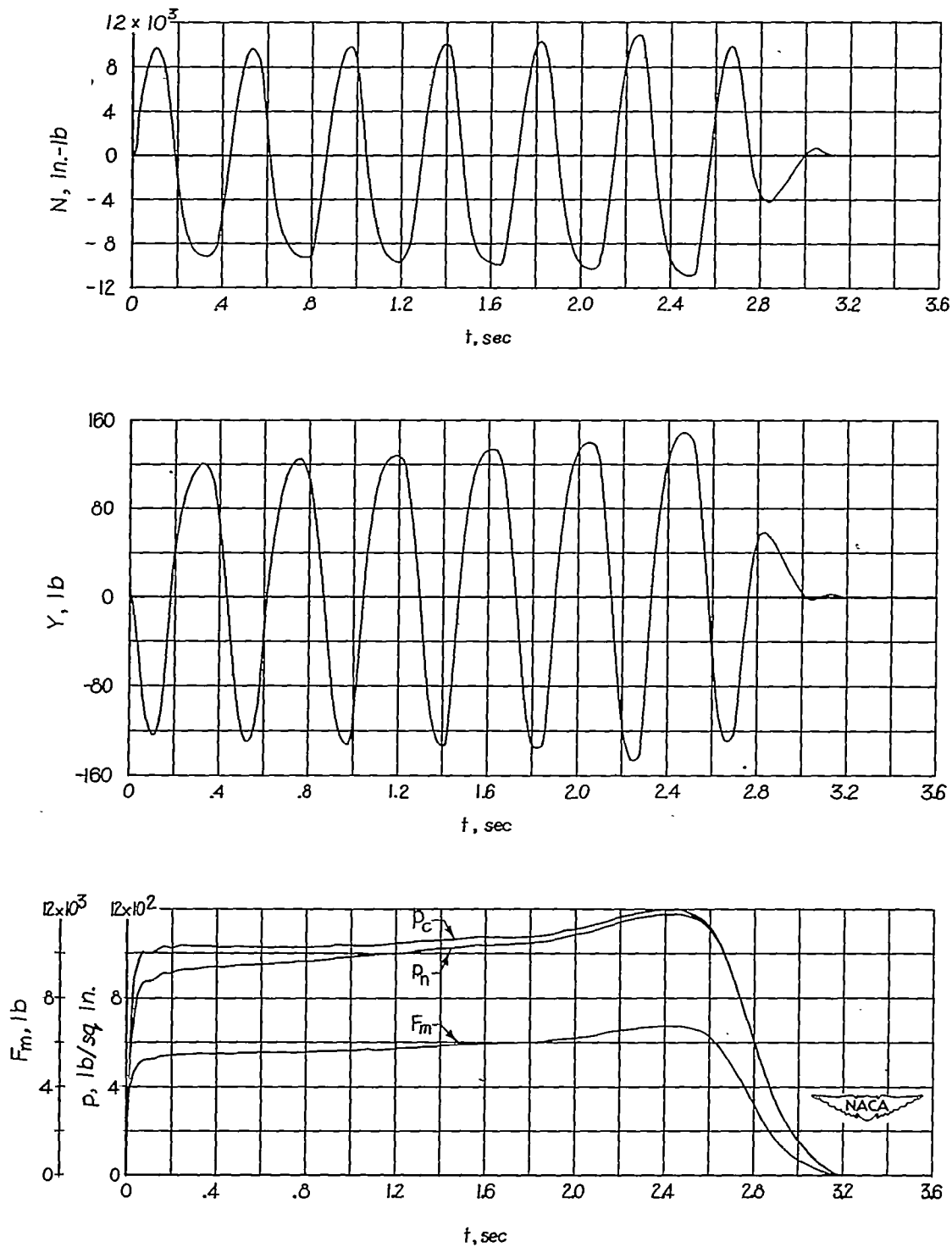
~~CONFIDENTIAL~~

Figure 9.- Time history of thrust-stand data obtained from test 3.

~~CONFIDENTIAL~~

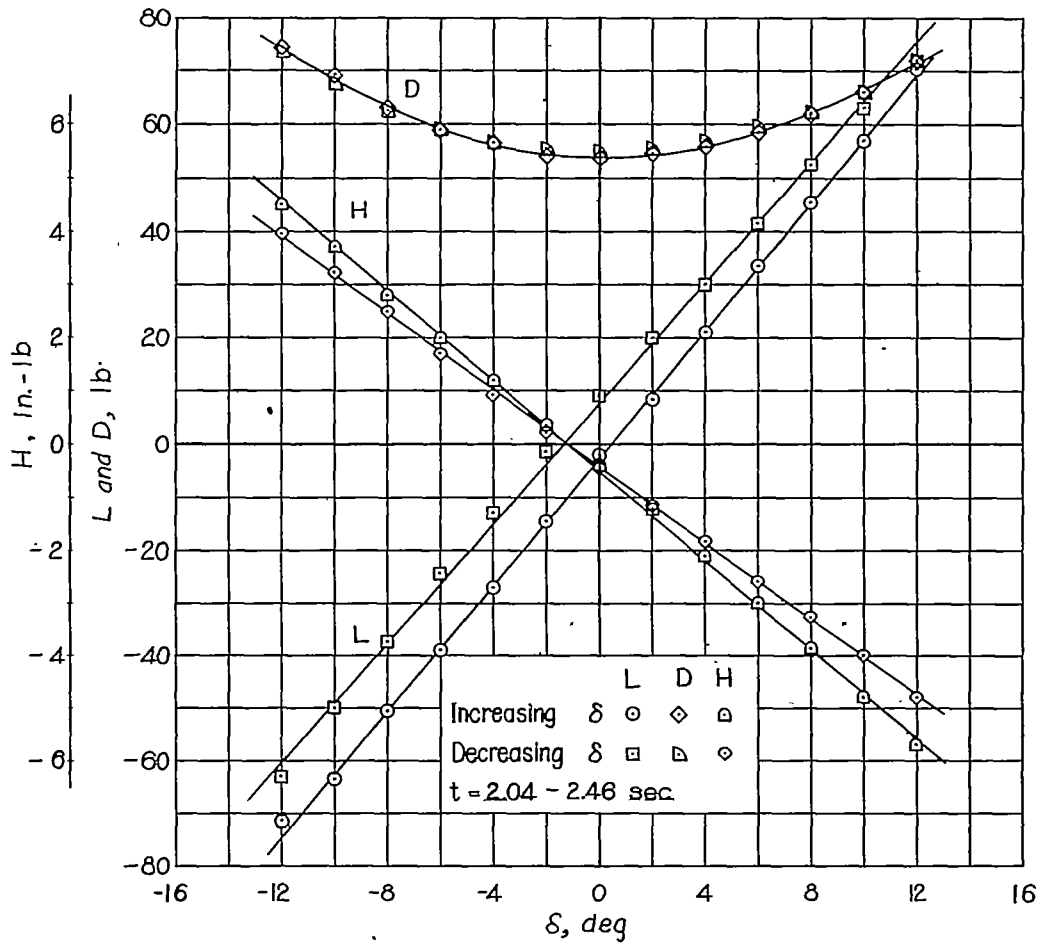


Figure 10.- Typical aerodynamic force characteristics from test 3.

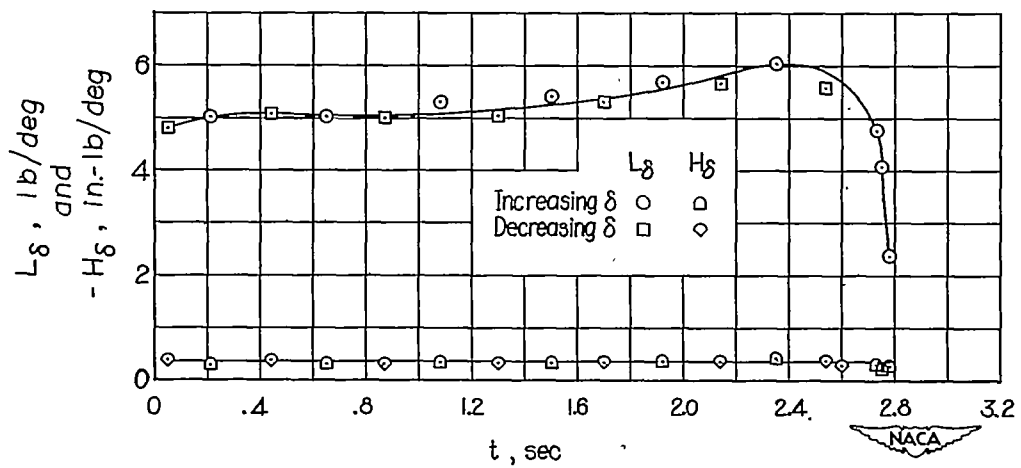


Figure 11.- Time history of L_δ and H_δ from test 3.

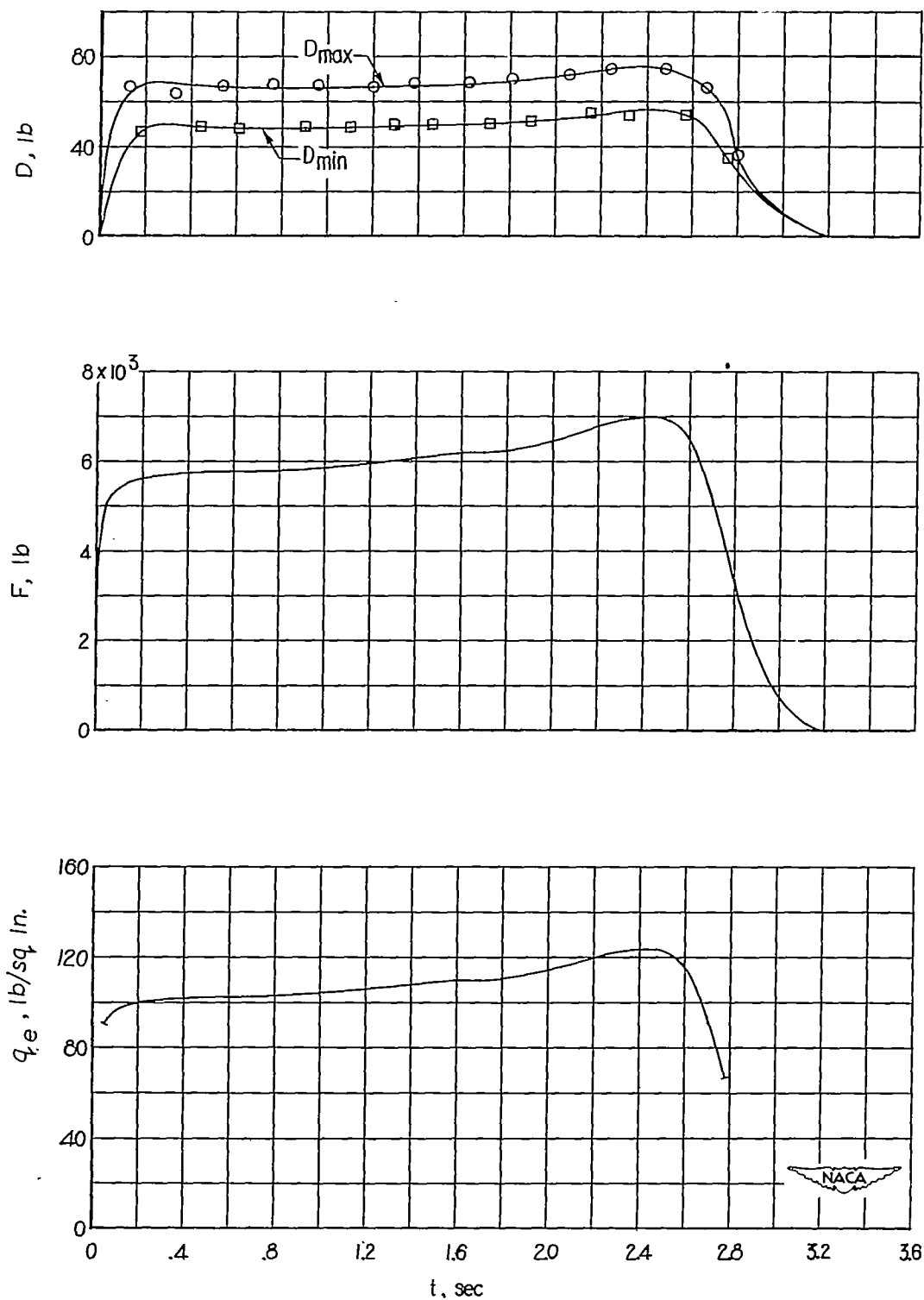


Figure 12.- Variation of D_{max} , D_{min} , thrust and dynamic pressure with time in test 3.

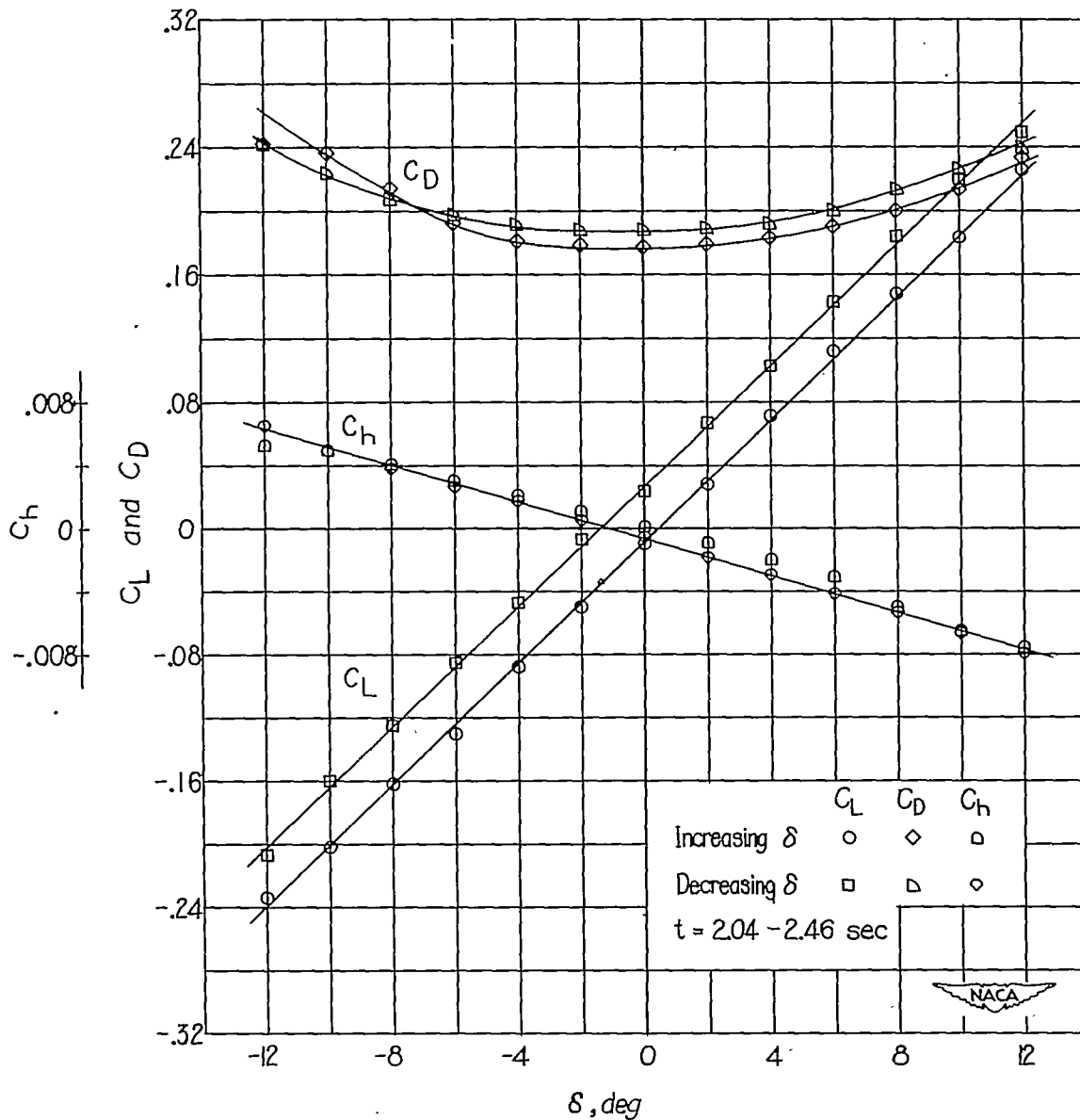


Figure 13.- Typical aerodynamic characteristics of jet vane obtained from test 3.

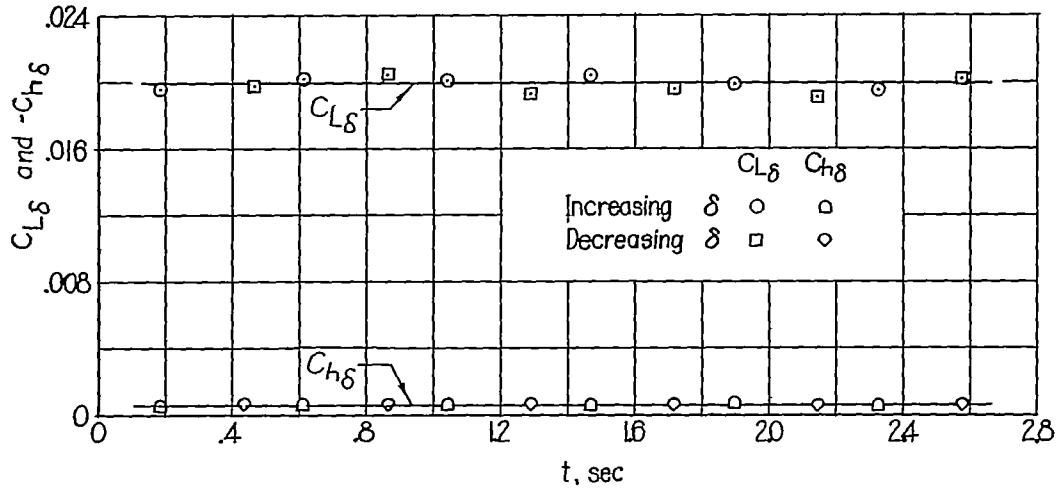


Figure 14.- Time history of $C_{L\delta}$ and $C_{h\delta}$ obtained from test 3.

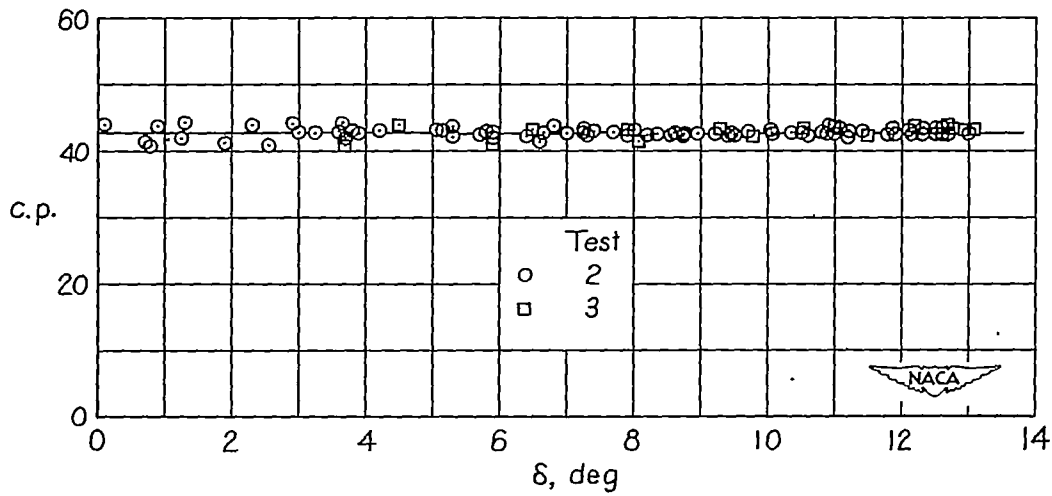


Figure 15.- Variation of center of pressure with vane deflection.